MICROROBOTS

# Enzyme-powered Janus platelet cell robots for active and targeted drug delivery

**Songsong Tang[1,2]*, Fangyu Zhang[1]*, Hua Gong[1]*, Fanan Wei[1], Jia Zhuang[1], Emil Karshalev[1], Berta Esteban-Fernández de Ávila[1], Chuying Huang[1], Zhidong Zhou[1], Zhengxing Li[1], Lu Yin[1], Haifeng Dong[2], Ronnie H. Fang[1], Xueji Zhang[2†], Liangfang Zhang[1†], Joseph Wang[1†]**



**Transforming natural cells into functional biocompatible robots capable of active movement is expected to enhance the functions of the cells and revolutionize the development of synthetic micromotors. However, present cell-based micromotor systems commonly require the propulsion capabilities of rigid motors, external fields, or harsh conditions, which may compromise biocompatibility and require complex actuation equipment. Here, we report on an endogenous enzyme-powered Janus platelet micromotor (JPL-motor) system prepared by immobilizing urease asymmetrically onto the surface of natural platelet cells. This Janus distribution of urease on platelet cells enables uneven decomposition of urea in biofluids to generate enhanced chemophoretic motion. The cell surface engineering with urease has negligible impact on the functional surface proteins of platelets, and hence, the resulting JPL-motors preserve the intrinsic biofunctionalities of platelets, including effective targeting of cancer cells and bacteria. The efficient propulsion of JPL-motors in the presence of the urea fuel greatly enhances their binding efficiency with these biological targets and improves their therapeutic efficacy when loaded with model anticancer or antibiotic drugs. Overall, asymmetric enzyme immobilization on the platelet surface leads to a biogenic microrobotic system capable of autonomous movement using biological fuel. The ability to impart self-propulsion onto biological cells, such as platelets, and to load these cellular robots with a variety of functional components holds considerable promise for developing multifunctional cell-based micromotors for a variety of biomedical applications.**

## INTRODUCTION

Evolved with distinctive features such as low immunogenicity, long life span, and binding specificity, natural cells have proven highly advantageous as carriers of therapeutic and diagnostic agents (*1*–*3*). For example, platelets are tiny, anucleate cells derived from the megakaryocyte of the bone marrow. Because of the relatively short life span of an individual platelet (around 8 to 10 days), billions of new platelets are produced daily to maintain normal platelet counts (*4*). The large volume and surface area of platelets facilitate efficient drug loading. With their combined abundancy, fast replenishment, high drug loading efficiency, and specific binding to biological threats, platelets have been considered an attractive platform for targeted drug delivery (*5*–*9*). However, vital cells, such as red blood cells (RBCs) and platelets, are immobile and rely on blood flow and passive diffusion to reach their desired destination, which may limit their overall binding, transport, and therapeutic efficacy when used as drug carriers. Transforming these passive cell systems into active and mobile delivery platforms is expected to open up new opportunities. Such a change in the operation of nanoscale systems from passive to active has been recently demonstrated with impressive benefits (*10*–*22*), including prolonged intestinal retention (*12*) and accelerated detoxification (*22*).

The use of micro/nanomachines that convert energy to propulsive force offers a viable route for realizing active cell-based delivery systems (*23*–*26*). Recent efforts toward cell-motor hybrid platforms can be classified into two main categories on the basis of the propulsion mechanism. The first category of cell robots relies on the propulsion by external fields, where cells are integrated with active components that respond to external stimulations (i.e., magnetic, acoustic, etc.) (*27*–*31*). Such externally propelled cell systems may experience constraints, such as the need for complex actuation equipment. The second category of cell-motor systems operates autonomously, relying on self-propelled micromotors interfaced with functional cells (*22*, *32*, *33*). For instance, natural cells such as RBCs and macrophages have been attached to bacteria or magnesium (Mg)–based micromotors, respectively (*22*, *33*). However, several concerns of biohybrid systems may limit their utility in practical clinical settings. For example, the pathogenicity and immunogenicity of bacteria may compromise the biocompatibility of bacteria-based platforms. Toxic propulsion fuels (e.g., $H_2O_2$) or short motor lifetimes (e.g., Mg-based micromotors) are additional barriers for diverse biomedical applications. Therefore, a fully biocompatible and biodegradable cell robot, capable of long-lasting self-propulsion in biological fuel, is highly desirable.

With the aforementioned design considerations, the use of enzymes to modify live cell motors represents an attractive approach, given their ability to convert their substrate biofuel into a driving force (*34*–*37*). Enzyme-based micro/nanomotors, relying on biocatalytic reactions of widely available biocompatible fuel substrates, can thus be used for practical biomedical applications. Such enzymes integrated onto micro/nanostructures can generate sufficient power in biological media containing their substrate fuel to overcome random Brownian motion and display efficient propulsion without requiring external fuels (*38*–*40*). Although early studies reported on the successful non-Janus modification of inorganic micro/nanospheres with enzymes to achieve propulsion (*37*, *41*–*43*), breaking the symmetry to obtain a Janus structure is essential for

[1]Department of NanoEngineering and Chemical Engineering Program, University of California San Diego, La Jolla, CA 92093, USA. [2]Research Center for Bioengineering and Sensing Technology, University of Science and Technology Beijing, Beijing 100083, China.
*These authors contributed equally to this work.
†Corresponding author. Email: josephwang@ucsd.edu (J.W.); zhang@ucsd.edu (L.Z.); zhangxueji@ustb.edu.cn (X.Z.)

achieving asymmetric driving force and generating efficient directional propulsion. The ability to immobilize enzymes onto cell surfaces has been proven viable for various applications (*44*–*46*), but reports on an active self-propelled cell motor based on enzyme modification of a cell surface in a Janus manner are scarce.

Here, we present urease-powered Janus platelet micromotors (JPL-motors) prepared by immobilizing the enzyme asymmetrically onto the surface of natural platelets (Fig. 1). As a major type of circulating blood cells, platelets offer multifunctionality in response to various microenvironments (i.e., hemostasis, inflammation, angiogenesis, wound healing, etc.) and specific binding to biological threats (cancer cells, bacteria, etc.) due to the versatile receptors on their surface (*4*, *47*, *48*). The JPL-motors developed in the present study leverage the intrinsic binding specificity and capacity of platelets to other biological subjects (*7*, *49*) for developing a new generation of targeted platelet micromotor powered by biocatalytic reactions of bioavailable fuels. By preserving the biological and structural features of regular platelets, the resulting JPL-motors have a wide range of platelet-like functions that other synthetic motors cannot achieve, for instance, specific binding and targeted delivery to cancer cells and bacteria.

The JPL-motors were fabricated by partially blocking the platelet surface through attachment of the platelets to a poly(L-lysine) (PLL)–modified surface in a commercial 12-well plate, followed by modifying the unblocked platelet surface with urease via a biotin-streptavidin-biotin binding complex (Fig. 1A). The biocatalytic reaction of the surface-bound urease in the presence of urea fuel generates an effective propulsion force through a chemophoretic mechanism. The resulting JPL-motors thus show efficient motion in diverse biological fluids in the presence of urea and significant propulsion enhancement in comparison with urease fully modified (non-Janus) platelets (denoted as "non-JPLs"), reflecting their asymmetrical structure. Our study demonstrates that the urease modification has a negligible effect on the functional proteins present on the platelet surface. This allows us to design a targeted platform on the basis of the intrinsic and specific binding of platelets to biological targets. The effective propulsion of the resulting JPL-motors in the presence of the urea fuel shows accelerated binding with cancer cells and bacteria and improved therapeutic efficacy of JPL-motors loaded with the model anticancer and antibiotic drugs, respectively. The integration of platelets with the urease biocatalytic engine enables the creation of an endogenous, biocompatible, and biodegradable cell robot that has the intrinsic properties of platelets along with the ability to self-propel. The cell surface engineering used for preparing the Janus urease coating represents a facile and robust method to asymmetrically functionalize the surface of natural cells. Such surface functionalization holds considerable potential for developing advanced cell robots. Using the body's own cellular materials as building blocks bestows the cell robots with capabilities to meet the rigorous properties required for biological applications, including superb biocompatibility, natural targeting ability, and high cargo-carrying capacity. These unique features would enable the cell robots for diverse biomedical applications including drug delivery, immunotherapy, and detoxification. Although the concept of creating enzyme-powered cell motors via an asymmetric biocatalytic cell coating has been presented here in connection to urease-modified platelet cells, it could be readily expanded for developing a multitude of self-propelled cell-based micromotors with diverse biofunctionalities based on different natural cells and enzyme modifications.

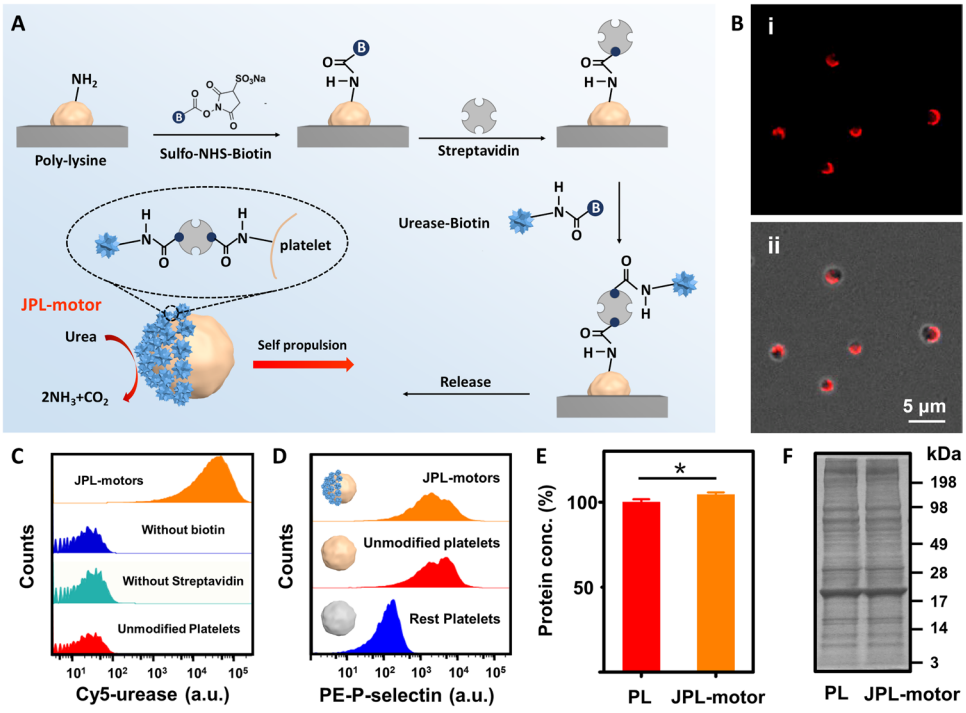


**Fig. 1. Fabrication and characterization of JPL-motors.** (**A**) Schematic of the fabrication of JPL-motors. Platelets were attached first to a PLL surface and then modified with urease via a biotin-streptavidin-biotin binding complex. (**B**) Fluorescent (i) and merged (ii) images of Cy5 and bright-field channels of JPL-motors with Cy5-labeled urease. (**C**) Representative flow cytometry histograms of Cy5-labeled urease under different conditions: JPL-motors (orange) and control experiments with unmodified platelets (red) and Janus modification of platelets without using biotin on urease (blue) or streptavidin (cyan). a.u., arbitrary units. (**D**) Representative flow cytometry histograms of the platelet activation marker P-selectin on JPL-motors (orange), unmodified platelets (red), and resting platelets (blue). (**E**) Quantification of the protein content of unmodified platelets (PL; red) and JPL-motors (orange) (both $5 \times 10^{11}$ cells/ml), stored in 1× PBS at 4°C for 24 hours. Error bars represent SDs from three independent measurements. The mean protein amount of unmodified platelets was normalized to 100% (*$P < 0.05$, *t* test). (**F**) SDS–polyacrylamide gel electrophoresis analysis of proteins presented on unmodified platelets (PL) and JPL-motors. The samples were run at equal protein content and stained with Coomassie blue.

## RESULTS

### Fabrication and characterization of JPL-motors

The JPL-motors were fabricated in a commercial PLL-modified 12-well plate. PLL is a positively charged amino acid polymer with lysine residues that are commonly used to coat tissue culture vessels to promote the nonspecific attachment of negatively charged cells or proteins through electrostatic interactions (*22*, *50*). To accomplish the asymmetric surface modification, platelets were attached first to

the PLL surface through centrifugation and further incubated for an hour. The centrifugation allowed partial platelet immersion into the PLL layer on the 12-well plate bottom, whereas the following incubation reinforced electrostatic attachment between the positively charged PLL surface and the negatively charged platelet membrane. This process enabled the partial blocking of the platelet membrane and allowed the subsequent Janus urease immobilization. As shown in Fig. 1A, the primary amines of the cell membrane proteins provided stable anchorage for cell surface engineering (*44*).

Then, sulfo–*N*-hydroxysuccinimide (NHS)–biotin, streptavidin, and urease-biotin were sequentially introduced to modify the platelet surface with urease (see Materials and Methods). Last, the resulting JPL-motors were dissociated from the PLL surface and suspended in phosphate-buffered saline (PBS) at 4°C until use. Using strong noncovalent binding interactions, the biotin-streptavidin-biotin complex provided a robust connection between the platelets and urease, ensuring high stability of the resulting cell robots in diverse biological environments.

The fabricated JPL-motors were characterized first by fluorescence microscopy using Cyanine5 [Cy5; excitation (Ex)/emission (Em) = 646/662 nm]–labeled urease. The optical and fluorescent images of JPL-motors with Cy5-labeled urease, shown in fig. S1 (A to C), demonstrate the monolayer distribution of JPL-motors on the well plate surface before pipetting. Further measurement of the JPL-motor sizes from the microscopy image of fig. S1A verified that about 82% of the JPL-motors are within a narrow size range of 1.4 to 2.6 μm (fig. S1D). The fluorescent image (i) of the Cy5 channel in Fig. 1B shows the Janus distribution of urease on JPL-motors. The merged image (ii) of the bright-field and Cy5 channels confirmed the effective localization of urease on JPL-motors and further verified the successful Janus modification of urease on platelet membranes as displayed by the asymmetric localization of the Cy5 fluorescent dye on the platelet surface. Moreover, the fabricated JPL-motors maintained the characteristic shape of platelets, revealing no damage to the cell morphology during the modification process or detachment of JPL-motors from the PLL substrate. The modification feasibility and efficiency of urease was further explored by flow cytometry analysis. As shown in Fig. 1C, around 96% of JPL-motors were Cy5 positive, whereas the Cy5 signal was not observed in control experiments involving unmodified PLs or Janus modification of platelets without using biotinylated urease or streptavidin. Such results further demonstrate the successful modification of urease on the JPL-motors. We also examined whether the JPL-motors remained as activated platelets, which is directly related to the inherent properties of platelets, such as their specific binding capability. Expression of P-selectin, a hallmark platelet activation marker, was thus evaluated among rest platelets (freshly isolated platelets without activation), unmodified but activated platelets, and JPL-motors. The results of flow cytometry analysis, displayed in Fig. 1D, reveal that the P-selectin expression for both unmodified PLs and JPL-motors was significantly enhanced in comparison with that of rest platelets, indicating that the platelets used for fabricating the JPL-motors were activated and unaltered by the urease modification. Furthermore, we investigated the effect of cell surface engineering on the protein content of JPL-motors. A bicinchoninic acid (BCA) protein assay was performed, as shown in Fig. 1E. The protein content of JPL-motors was slightly higher than that of unmodified PLs at the same cell concentration ($5 \times 10^{11}$ cells/ml), which may be ascribed to the additional molecules (i.e., biotin) and proteins (i.e., streptavidin and urease) on the JPL-motor membrane. On the basis of the protein quantification, we also estimated the amount of urease per JPL-motor, which corresponds to 136 ± 25 molecules. Details of these calculations are given in the Supplementary Materials. Gel electrophoresis analysis of Fig. 1F illustrates that the protein profile of JPL-motors matches closely to that of unmodified PLs at the same protein concentration. However, the bands of the attached streptavidin or urease moieties cannot be found in the gel electrophoresis analysis because of their significantly lower amounts compared with those of proteins existing on the platelet surface. These results demonstrate that the platelet surface can be modified with urease without altering its protein profile, which is a prerequisite for subsequent biomedical applications of JPL-motors.

## Propulsion performance of JPL-motors and non-JPLs

The Janus distribution of urease over the platelet surface results in asymmetric biocatalytic decomposition of urea into ammonia and carbon dioxide, as illustrated in Fig. 1A and the following Eq. 1:

$$(NH_2)_2CO + H_2O \xrightarrow{urease} CO_2 + 2NH_3 \quad (1)$$

Subsequently, a concentration gradient and active directional flow of reaction products around JPL-motors are generated, which drives the JPL-motor to undergo self-diffusiophoretic propulsion. The propulsion data were acquired by optical tracking of individual micromotor samples. Figure 2A (and corresponding movie S1) displays the typical tracking trajectories of JPL-motors in the presence of varying urea concentrations (0, 50, 100, and 200 mM) in PBS and illustrates the enhanced motion with increasing urea fuel concentrations. The propulsion of multiple JPL-motors in the presence of 50 mM urea is also demonstrated in movie S2. On the basis of the *X*-*Y* coordinates of the micromotor trajectories, taken from the optical tracking, the mean-squared displacement (MSD) was calculated as a function of the time interval ($\Delta t$) along with different concentrations. In Fig. 2B, the MSD increases linearly with time in low fuel concentration. This behavior changed at higher urea concentrations (100 and 200 mM), starting off as linear and shifting to parabolic, reflecting the effective directional motion of the cell robots under these conditions. Aiming at using JPL-motors in practical biomedical applications, we also examined the propulsion behavior of the motors in biologically relevant environments. As illustrated in Fig. 2C (and corresponding movie S3), the motion behavior of the cell robots in Dulbecco's modified Eagle medium (DMEM), blood, and simulated urine in the presence of 100 mM urea is comparable with their movement in PBS. The effective diffusion coefficient ($D_{eff}$) was estimated by fitting the MSD curves to Eq. 2

$$MSD(\Delta t) = 4 D_{eff} \Delta t \quad (2)$$

where $D_{eff}$ represents the effective diffusion coefficient and $\Delta t$ represents the time interval (*51*, *52*). The corresponding $D_{eff}$ is shown in Fig. 2D. Such propulsion behavior of the JPL-motors in various media further demonstrates the robustness of the Janus modification under different conditions toward expanded possibilities in diverse environments. We also explored the propulsion behavior of unmodified PLs in aforementioned biological fluids containing 100 mM urea. As expected, in the absence of immobilized urease engine, only a Brownian motion was observed in the different media (fig. S2 and movie S4). Because the Brownian motion is affected only

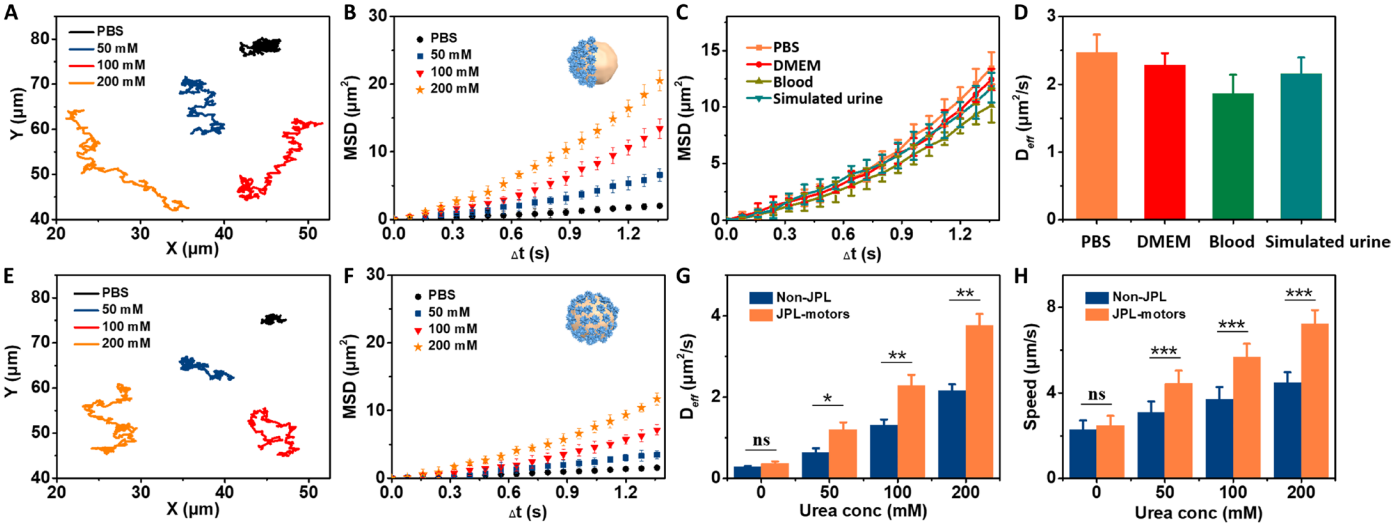


**Fig. 2. Motion behavior of JPL-motors and urease fully modified platelets (non-JPLs).** (**A**) Optical tracking trajectories (over 20 s) and (**B**) MSD of JPL-motors in PBS solution with different urea concentrations [$n = 15$; mean ± standard error of the mean (SEM)]. (**C**) MSD and (**D**) corresponding $D_{eff}$ of JPL-motors in various media at the same urea concentration (100 mM) ($n = 15$; mean ± SEM). (**E**) Optical tracking trajectories (20 s) and (**F**) MSD of the non-JPLs in PBS solution with different urea concentrations. Comparisons of the (**G**) $D_{eff}$ ($n = 15$; mean ± SEM) and (**H**) speed ($n = 15$; mean ± SD) of JPL-motors and non-JPLs in the presence of different urea concentrations. *$P < 0.05$, **$P < 0.01$, and ***$P < 0.001$; ns, no statistical significance; *t* test.

by the temperature and the viscosity of the fluid, the unmodified PLs (lacking the urease engine) are expected to display Brownian motion independent of the presence of urea. We also examined the lifetime of the JPL-motors. As shown in fig. S3 (movie S5), the JPL-motors still displayed effective propulsion after 30 min at a urea concentration of 100 mM compared with their initial motion. Such biocatalytic propulsion with long life span holds great potential for addressing the requirement of practical applications. The observed path decrease is largely due to the depletion of the urea fuel, whereas the slow translational diffusion of the attached urease enzymes on cell membrane might also contribute to the path decrease by breaking the asymmetric enzyme distribution on the JPL-motors.

Several studies have reported that non-Janus coating of enzymes on polystyrene particles (*37*) or mesoporous silica nanoparticles (*41*–*43*) could enhance diffusive motion due to the unbalanced distribution of enzymes on the surface. Here, non-JPLs were also fabricated (see Materials and Methods) to compare their propulsion behavior with that of JPL-motors. The characterizations of non-JPLs with Cy5-labeled urease are presented in fig. S4. The fluorescence intensity of Cy5-labeled urease can be observed uniformly over the surface of the platelets (fig. S4, A to C). The successful fabrication of non-JPLs is further confirmed by flow cytometry analyses shown in fig. S4D, demonstrating that the non-JPLs display a strong Cy5 signal (~99%) compared with the unmodified PLs. Compared with the images shown in Fig. 1B, such results further validated our methodology for Janus cell surface engineering. The optical tracking trajectories and calculated MSD of non-JPLs were shown in Fig. 2 (E and F, respectively) (movie S6), where an increase in displacement was observed upon increasing the urea concentration. However, as expected, JPL-motors displayed a more efficient propulsion and larger MSD compared with the corresponding non-JPLs. This difference was attributed to the asymmetric propulsion force generated by JPL-motors and was further confirmed by the $D_{eff}$ and speed. Figure 2G compares the calculated $D_{eff}$ of JPL-motors and non-JPLs. Although no major difference was observed in the absence of fuel, in the presence of urea, the $D_{eff}$ of JPL-motors was approximately two times higher compared with that of non-JPLs at the same fuel concentration. A similar trend was observed in Fig. 2H when comparing the speed obtained from optical tracking, with the JPL-motors displaying a higher speed (1.62-fold) than non-JPLs at 200 mM urea. Overall, these results demonstrate that JPL-motors exhibit effective movement in various biological media in the presence of urea and enhanced propulsion compared with non-JPLs, reflecting the stronger net propulsion force generated by the asymmetric enzyme distribution on the cell surface.

## In vitro anticancer drug delivery of JPL-motors

The successful fabrication of JPL-motors and their effective propulsion in diverse biological fluids allowed us to investigate their use in biological applications. Considering that platelets play crucial roles in cancer metastasis, including interacting directly with cancer cells (*47*), the active targeted JPL-motor platform holds great potential to improve drug delivery to cancer cells. Here, the breast cancer cell MDA-MB-231, known for its interaction with platelets (*53*), was used as a model to evaluate the anticancer activity of chemodrug-loaded JPL-motors (Fig. 3A). We first examined the specific adhesion of JPL-motors to cancer cells. Figure 3B presents a scanning electron microscope (SEM) image illustrating the adhesion and aggregation of JPL-motors (pseudocolored in pink) on an MDA-MB-231 cell (pseudocolored in purple) after 10 min of incubation at a urea concentration of 100 mM. Such specific binding is also demonstrated by fluorescent microscopy. JPL-motors and MDA-MB-231 cells were labeled with Cy5 and Hoechst 33342 (Ex/Em = 361/497 nm) dyes, respectively. Figure 3C shows the bright-field (i) and fluorescent (ii to iv) images of JPL-motors (iii, red) attached onto an MDA-MB-231 cell (ii, blue). The adhesion of cancer cells with PLs and RBCs has been used as positive and negative controls, respectively, to further explore the effect of the urease modification on the binding affinity

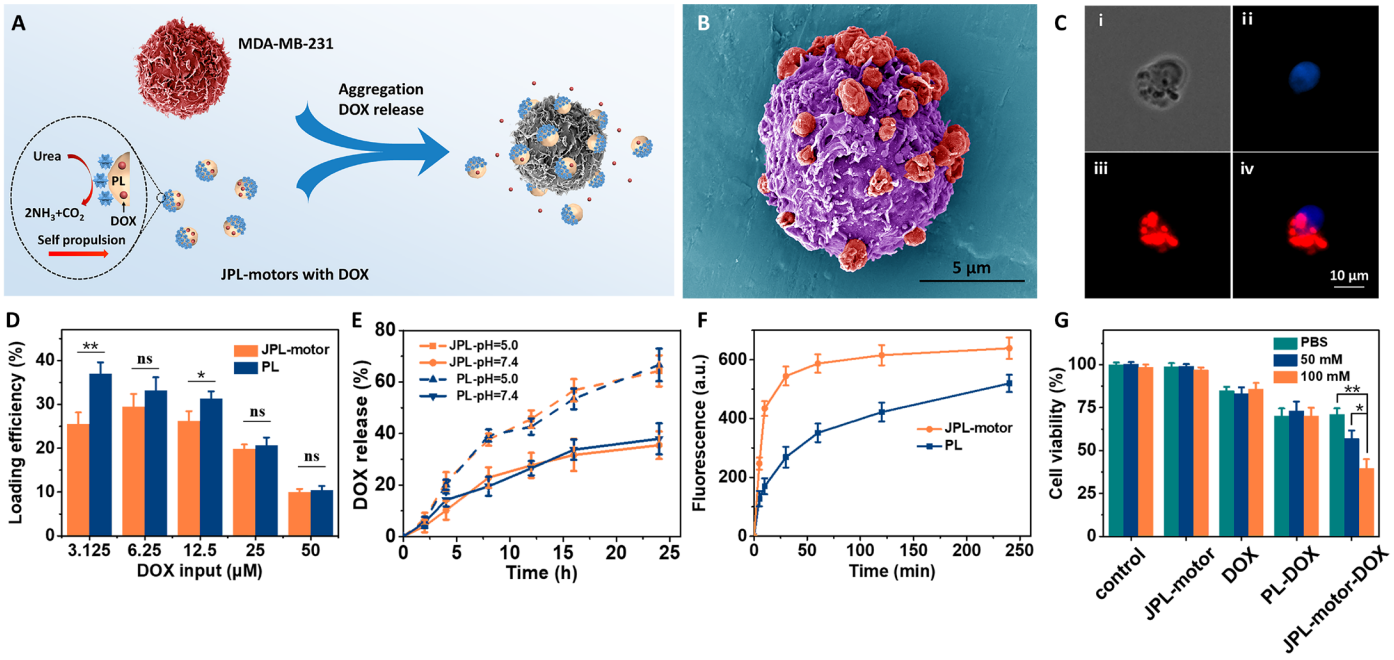


**Fig. 3. Enhanced binding and anticancer activity of chemodrug-loaded JPL-motors.** (**A**) Schematic of JPL-motor–DOX for cancer-targeted delivery. MDA-MB-231 breast cancer cells were selected as a model cell line. (**B**) Pseudocolored SEM image of numerous JPL-motors (red) attached to an MDA-MB-231 cell (purple). (**C**) Bright-field (i) and fluorescent (ii to iv) images showing the binding between an MDA-MB-231 cell and JPL-motors, labeled with Hoechst 33342 (ii, blue) and Cy5 (iii, red), respectively. Overlay of the two channels is shown in (iv). (**D**) Loading efficiency of JPL-motors and unmodified platelets (PLs) at various DOX initial inputs ($n = 3$; mean ± SD). $^*P < 0.05$ and $^{**}P < 0.01$, *t* test. (**E**) Cumulative release of DOX from DOX-loaded JPL-motors and unmodified platelets (PLs) at pH 5.0 or 7.4 over 24 hours ($n = 3$; mean ± SD). (**F**) Comparison of the fluorescence intensity of MDA-MB-231 cells after incubation with DiD-labeled JPL-motors or unmodified platelets (PLs) over different periods of time at 100 mM urea ($n = 3$; mean ± SD). (**G**) Viability of MDA-MB-231 cells after incubation with control solutions (only PBS or urea), JPL-motors, free DOX, PL-DOX, and JPL-motor–DOX at the same DOX concentration of 10 μM at various urea concentrations (0, 50, and 100 mM) for 10 min and separated for another 24 hours of incubation ($n = 3$; mean ± SD). $^*P < 0.05$ and $^{**}P < 0.01$, *t* test.

of platelets. JPL-motors, PLs, and RBCs have thus been labeled with 1,1′-dioctadecyl-3,3,3′,3′-tetramethylindodicarbocyanine (DiD; Ex/Em = 648/668 nm) and incubated for 30 min with MDA-MB-231 cells at the ratio of 10:1, followed by flow cytometry analysis. As shown in fig. S5, both the JPL-motors and PLs displayed comparable DiD positive (~96%), whereas no DiD signal was observed for the negative RBC control. These data demonstrate that the enzyme modification of JPL-motors has no influence on the intrinsic adhesion properties of platelets, which is in agreement with the results of Fig. 1D and allows the design of JPL-motor–based targeted delivery platforms.

After confirming the specific binding capability of JPL-motors with MDA-MB-231 cells, the antitumor efficacy of drug-loaded JPL-motors was evaluated. Doxorubicin (DOX), a widely used chemotherapeutic drug, was selected for this study. The drugs are expected to be loaded onto the platelet cell through both electrostatic absorption and cellular endocytosis (*54*–*56*). Initially, the capability of JPL-motors to load DOX was confirmed by fluorescent microscopy (fig. S6). Then, the loading capacity was explored with increasing inputs of DOX. In Fig. 3D and fig. S7, JPL-motors showed comparable loading capacity to unmodified PLs, indicating that the surface modification only has a slight effect on drug encapsulation. The maximum loading amount was obtained with 25 μM input concentration of DOX (fig. S7), corresponding to a 20% loading efficiency per $10^8$ cells (Fig. 3D), whereas larger DOX concentrations provided lower loading efficiencies. We also explored the propulsion behavior of DOX-loaded JPL-motors. Only slight differences in trajectory and MSD were observed between DOX-loaded JPL-motors and unloaded JPL-motors (fig. S8 and movie S7), reflecting the effective propulsion of the drug-loaded cell robot platform. Subsequently, the DOX release from JPL-motors was analyzed over 24 hours at two different pH values. The JPL-motors displayed a similar and comparable DOX release behavior compared with PLs (Fig. 3E). The enhanced DOX release within 24 hours at a lower pH 5.0, compared with that at the physiological pH 7.4, might be due to the destabilization and protein denaturation of the platelet membrane at a lower pH value (*57*). Enhanced release at low pH may facilitate effective drug delivery to tumors with their acidic microenvironments. Before evaluating the anticancer efficacy of DOX-loaded JPL-motors, the binding efficiency of cancer cells with JPL-motors or unmodified PLs was analyzed. Both JPL-motors and unmodified PLs were labeled with DiD and then incubated with MDA-MB-231 cells at 100 mM urea for different periods (5 min, 10 min, 30 min, 1 hour, 2 hours, and 4 hours). The optimized centrifugation speed of 100 relative centrifugal force (rcf) per minute was chosen to isolate the resulting aggregates from the free JPL-motors, PLs, and cancer cells. Then, the fluorescence intensity of DiD was measured. A rapid increase in fluorescence was observed within 30 min for JPL-motors, followed by a gradual saturation in signal (Fig. 3F). In contrast, MDA-MB-231 cells cultured with unmodified PLs showed a much slower fluorescent signal increase, demonstrating that the active motion can accelerate the specific adhesion between JPL-motors and cancer cells. The incubation time with the maximum difference of binding efficiency was 10 min,

where the fluorescence intensity of DiD in JPL-motors reached a 2.55-fold increase compared with that of passive unmodified PLs. Subsequently, anticancer efficacy was evaluated on the basis of the optimized incubation time. Figure 3G displays the viability of MDA-MB-231 cells cultured at various conditions for 10 min and then isolated for another 24 hours of incubation. Three urea concentrations (0, 50, and 100 mM) were examined for each condition. Incubation with PBS or urea only (control in Fig. 3G) and JPL-motors without DOX loading (JPL-motor in Fig. 3G) were performed as negative controls and resulted in a negligible influence on cell viability, indicating the biocompatibility of JPL-motors and their propulsion fuel. When treated with free DOX, cancer cells displayed around 80% cell viability (DOX in Fig. 3G). Lower viability (~70%) was observed for MDA-MB-231 cells treated with DOX-loaded unmodified PLs (PL-DOX in Fig. 3G). It is also shown that different urea concentrations have negligible effects on cell growth for both free DOX and PL-DOX groups. In comparison, cells treated with DOX-loaded JPL-motors (JPL-motor–DOX in Fig. 3G) exhibited a substantial decrease in viability upon increasing the urea concentration. Forty percent cell viability was achieved at 100 mM urea, which is a 1.75-fold decrease compared with PL-DOX. The effective propulsion of JPL-motors thus accelerated their binding with cancer cells and enhanced local DOX concentration for improved anticancer effects (Fig. 3G). Overall, these results demonstrate that our cell robot therapeutic platform, with self-propulsion in the presence of urea, is capable of accelerating specific adhesion to cancer cells and enhancing anticancer efficacy.

### In vitro antibacterial drug delivery of JPL-motors

Encouraged by the enhanced anticancer efficacy of DOX-loaded JPL-motors, we explored whether this active therapeutic platform could be generalized to other payloads and biological threats. Here, we investigated the potential antibacterial application of JPL-motors by taking advantage of the platelets' high binding affinity to certain bacteria (*49*, *58*). We chose *Escherichia coli*, known to bind to platelets (*59*), as the model bacteria to assess the JPL-motor–bacterium interactions (Fig. 4A). Figure 4B displays an SEM image of the adhesion between a JPL-motor (pseudocolored in green) and *E. coli* (pseudocolored in pink) after 5 min of incubation at 100 mM urea. The platelet aggregation induced by *E. coli* was also shown in fig. S9. To further verify the motor-bacterium binding, we labeled the JPL-motors and *E. coli* with Cy5 and 4′,6-diamidino-2-phenylindole (DAPI; Ex/Em = 358/461 nm), respectively. The bright-field (i) and fluorescent images (ii to iv) of the *E. coli* (ii, blue) and JPL-motor (iii, red) aggregates are shown in Fig. 4C, revealing the binding affinity between *E. coli* and the cell robots. We further quantified the specific binding of JPL-motors with *E. coli* along with the binding to PLs serving as control. Both JPL-motors and PLs (labeled with DiD) were incubated with *E. coli* (labeled with DAPI) for 30 min at the ratio of 1:5. The binding percentage was estimated by manually counting 10 representative images taken from each sample. As shown in fig. S10, only a slight difference in the binding level is observed for both JPL-motors and PLs, indicating that the Janus modification has a negligible influence on the binding affinity of platelets to bacteria. The demonstrated binding ability of the JPL-motors to

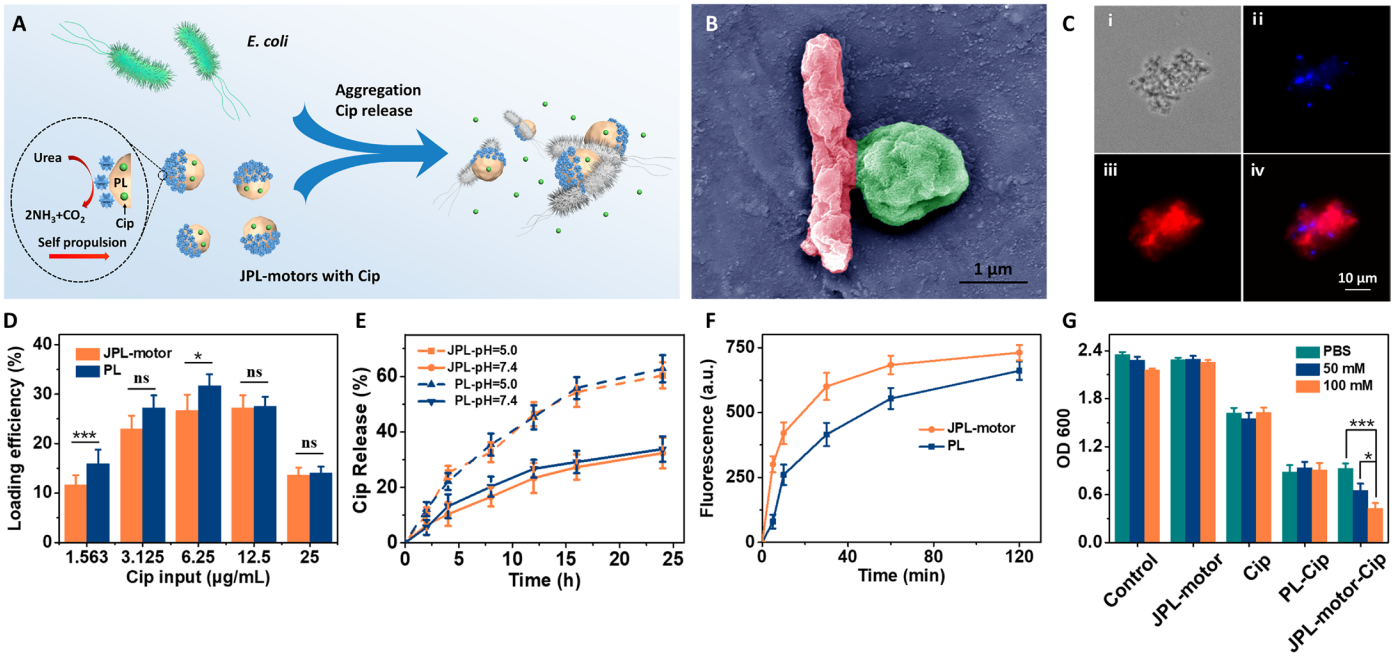


**Fig. 4. Enhanced binding and antibacterial activity of antibiotic-loaded JPL-motors.** (**A**) Schematic of JPL-motor–Cip for bacterium-targeted delivery. *E. coli* was selected as a model bacterium. (**B**) Pseudocolored SEM image of the binding between the JPL-motor (green) and *E. coli* (red). (**C**) Bright-field (i) and fluorescent (ii to iv) images of the binding between *E. coli* and JPL-motors, labeled with DAPI (ii, blue) and Cy5 (iii, red), respectively. The merged image of two channels is shown in (iv). (**D**) Loading efficiency of JPL-motors and unmodified platelets (PLs) at various Cip initial inputs ($n = 3$; mean ± SD). $^*P < 0.05$ and $^{***}P < 0.001$, *t* test. (**E**) Cumulative released percentage of Cip from Cip-loaded JPL-motors and unmodified platelets (PLs) at pH 5.0 or 7.4 over 24 hours ($n = 3$; mean ± SD). (**F**) Comparison of fluorescence intensity of *E. coli* after incubation with DiD-labeled JPL-motors or unmodified platelets (PLs over different periods of time at 100 mM urea) ($n = 3$; mean ± SD). (**G**) $OD_{600}$ of *E. coli* after culture with control solutions (only PBS or urea), JPL-motors, free Cip, PL-Cip, and JPL-motor–Cip at the same Cip concentration of 10 μg/ml at various urea concentrations (0, 50, and 100 mM) for 5 min and separated for another 24 hours of incubation ($n = 3$; mean ± SD). $^*P < 0.05$ and $^{***}P < 0.001$, *t* test.

cancer cells and bacteria relies on the numerous protein receptors on the surface of platelets. For example, bacteria can bind with the platelet Toll-like receptors, leading to the activation and aggregation of platelets (*49*, *58*). Platelet receptors, such as αIIbβ3, P-selectin, and α6β1, are responsible for the PL binding with cancer cells (*47*). These biological receptor-ligand interactions enable the recognition and binding of platelets to the target cells. Because platelets express many unique functional receptors on its membrane that other cells, such as RBCs, do not express, our JPL-motors are expected to target a wide range of biological threats that have binding affinity with platelets.

Ciprofloxacin (Cip), an antibiotic used to treat a wide variety of Gram-negative bacterial infections (*60*), was used for antibacterial evaluation. The drug loading capacity was first analyzed. The loading amount of JPL-motors increased with the Cip input, reaching the maximum loading at 12.5 μg/ml input concentration of Cip (fig. S11), corresponding to a loading efficiency of ~27% (Fig. 4D). Increasing the Cip input to 25 μg/ml resulted in a smaller loading efficiency. It was also observed that Cip-loaded JPL-motors exhibited propulsion comparable with their unloaded counterparts (fig. S12 and movie S8). Subsequently, Cip release was measured over 24 hours at two pH values (Fig. 4E). Similar to the DOX formulation, JPL-motors and PLs exhibit a negligible difference in the amounts of released Cip at each pH value. Moreover, at pH 5.0, both JPL-motors and PLs displayed a nearly twofold higher Cip release compared with pH 7.4. The binding efficiency of JPL-motors or PLs to *E. coli* was also explored. DiD-labeled JPL-motors or unmodified PLs were cultured with *E. coli* at 100 mM urea for different incubation times, followed by centrifugation at an optimized centrifugation speed of 600 rcf/min and washing steps to separate the resulting aggregates and remove the free JPL-motors or unmodified PLs. The increase of DiD fluorescence intensity in the aggregates was measured and calculated in the same way as above. JPL-motors induced a rapid fluorescence increase in comparison with non-JPLs (Fig 4F). The maximum difference in signal was achieved at 5 min, which was chosen as the incubation time for the following antimicrobial efficacy evaluation. This difference is attributed to the active motion of JPL-motors, leading to rapid adhesion to *E. coli*. To test the antibacterial effectiveness, an *E. coli* suspension [$2 \times 10^5$ colony-forming units (CFU) per milliliter] was incubated with free Cip (Cip in Fig. 4G), unmodified PLs loaded with Cip (PL-Cip in Fig. 4G), and JPL-motors loaded with Cip (JPL-motor–Cip in Fig. 4G) at the same drug concentration (10 μg/ml) with different urea concentrations for 5 min. The bacteria were then collected through centrifugation and transferred to fresh LB broth for a subsequent 24-hour incubation. The negative controls were also performed by mixing *E. coli* with PBS or urea only (control in Fig. 4G) or JPL-motors without Cip (JPL-motor in Fig. 4G), revealing a negligible effect on bacteria colonization. Only JPL-motors display a urea concentration–dependent bacteria inhibitory effect with the lowest optical density (0.4) at 600 nm ($OD_{600}$) with 100 mM urea, which is around 3.6- and 2.1-fold lower than that of Cip and PL-Cip, respectively. The significant antibacterial effect of JPL-motors reflects their self-propulsion in the presence of urea, which accelerates adhesion to bacteria and induces higher local Cip concentrations. Overall, these results indicate that the effective propulsion and the specific binding of our cell robots to bacteria significantly improve their antibacterial efficacy compared with passive systems.

## DISCUSSION

Several challenges facing existing cell robot systems may hinder their practical use for biomedical applications. The first concern for biohybrids is biocompatibility. For example, live bacterium–driven microswimmers may induce an immune response (*33*). The second issue is the potential toxicity of the propulsion fuel, for instance, the use of $H_2O_2$ during the manipulation of breast cancer cells (*32*). Thus, there is demand for alternative biocompatible platforms and fuels to expand the biomedical prospects of micromotors. Another challenge in the application of biohybrid micromotors in biological environments is the limited motor life span. Despite good biocompatibility and biodegradability of Mg-based biohybrid micromotors, they still suffer from a short lifetime (~2 min), which compromises their application in certain environments (*12*, *22*, *61*). On the other hand, although fuel-free propulsion mechanisms, based on the use of external acoustic or magnetic fields, have shown impressive performance in actuating and controlling micromotors for in vivo tests, these systems require relatively complex actuation systems and have limited tissue penetration. To overcome these limitations, we have demonstrated a platelet cell robot powered by urease with autonomous and long-lasting propulsion in the presence of urea, triggered by the corresponding enzymatic fuel decomposition that obviates the need for motor actuation. The integration of the endogenous enzyme with platelet cells yields a fully biocompatible cell robot system. The biofunctionality of platelet cells combined with an efficient motor results in an attractive platform with unique synergistic capabilities that can be useful for a broad range of biomedical applications. Moreover, the urea fuel is a common biological substrate readily available in the body, especially in the urinary system, making these types of microenvironments an attractive choice for initial clinical investigation. The methodology developed here leads to a facile and robust route to asymmetrically modify cell surfaces with urease. The Janus structure is highly preferable for achieving asymmetric driving force and active motion compared with complete enzymatic coverage of the entire cell membrane. The current Janus cell modification was realized by attaching platelets onto a PLL-modified substrate to block the attached platelet surface and modifying the exposed cell membrane with urease via a biotin-streptavidin-biotin binding interaction. The asymmetric distribution of urease on JPL-motors, demonstrated by fluorescent imaging using Cy5-labeled urease, results in an asymmetric propulsion force and leads to greatly enhanced movement in the presence of urea compared with non-JPLs. The ability to overcome Brownian motion and achieve effective propulsion enables the integration of asymmetrically engineered platelets into the microrobotic community to expand the design, functionality, and versatility of microrobots on the basis of the Janus modification and intrinsic properties of platelets (*14*). The cell surface engineering route has a negligible effect on the functional proteins of platelet membrane, endowing JPL-motors with the unique capabilities of drug loading and specific binding to biological threats. The effective propulsion of JPL-motors in the presence of urea significantly enhances their binding efficiency to cancer cells and bacteria, and this, in turn, improves the in vitro therapeutic efficacy compared with passive unmodified PLs. These improvements can lead to decreased drug dosages, which can ultimately reduce unwanted side effects. Cell surface engineering transforms cells into active micromotors and can be readily generalized to other types of cells (e.g., RBCs and T cells) or enzymes (e.g., catalase and glucose oxidase) to open up a wide range of new biomedical opportunities.

The findings from this work illustrate a concept of using enzyme asymmetrically modified natural cells as live cellular robots for active and targeted delivery. The platform combines the merits of biocompatibility and functions of natural cells with active propulsion ability empowered by biological enzymes. In terms of potential medical applications, these cell robots can be readily expanded to carry other types of therapeutic or diagnostic payloads or to achieve a mission other than active delivery such as biodetoxification. The production and regulation of urea are crucial for various metabolic processes in the human body. The normal urea concentration in human blood ranges from 2.5 to 6.5 mM. In other biofluids, such as urine, the level of urea is significantly higher. Despite the large urea fluctuations in urine (ranging from 102 to 835 mM), this biofluid is particularly suitable for the propulsion of JPL-motors. The bioavailable propulsion fuel of the JPL-motors makes the platform amenable to future biomedical applications such as treatment of urinary tract infection or bladder cancer. Although the ammonia product of the biocatalytic decomposition of urea may contribute to a higher local pH and potential cytotoxic effect, such effects were reported to be controllable by adjusting the input of urease-powered micromotors for in vitro bladder cancer therapy (*42*). This study demonstrated the safe in vivo application of urease-powered micromotors for bladder cancer treatment using an optimized motor concentration displaying low toxicity. Future in vivo studies and applications will require precise control to manipulate the cell robots to perform complex tasks in dynamic environments. Coupled with new functionalization and propulsion strategies, real-time tracking and imaging of the cell robots inside the body remain challenges that need to be addressed in parallel to the development of cell robots. In addition, directional movement of living cells induced by chemotaxis is critical for practical applications in biological systems (*62*). Investigating the effect of concentration gradients of substrates on the propulsion of Janus cell robots holds considerable potential for designing multifunctional platforms with autonomous movement in response to complex environments. Overall, the Janus modification of cell surfaces offers an inspiring and versatile avenue for transforming passive cells into active cell robots. Such a strategy paves the way for efficient biocompatible cell robot platforms that meet the rigorous requirements of clinical biomedical applications.

## MATERIALS AND METHODS

### Preparation of urease-biotin-Cy5

Urease (Sigma-Aldrich) was first dissolved in PBS (1×; pH 7.4) at 1 mg/ml. Sulfo-NHS-biotin (200 μl; 16.6 μM; ProteoChem) was then mixed with urease solution (200 μl, 1 mg/ml) and reacted for 30 min with gentle shake at room temperature. Subsequently, 4 μl of sulfo-Cy5 NHS ester (sulfo-NHS-Cy5; 1 mM; Lumiprobe) was added for another 30-min incubation. Last, the modified urease was purified four times with PBS through a 100-kDa filter (Millipore) with centrifugation at 1500 rcf for 3 min. The resulting urease-biotin-Cy5 was dispersed in 400 μl of PBS and stored at 4°C until use.

### Fabrication of JPL-motors

Human platelets were purified from platelet-rich plasma (San Diego Blood Bank). JPL-motors were prepared in commercial 12-well plates modified with PLL (Corning). Platelets ($10^9$ cells) suspended in 400 μl of PBS were added to a 12-well plate and spun down to the PLL surface with a 3-min centrifugation at 900 rcf. After 1 hour of incubation at room temperature, the supernatant was removed and the plate was washed three times with PBS to remove all the unattached platelets. Afterward, the attached platelets were reacted with sulfo-NHS-biotin (166 μM), streptavidin (ProSpec; 166 μM), and urease-biotin-Cy5 (described above) for 1 hour, respectively. Three washes with PBS were needed for the removal of free agents between each reaction. Last, the resulting JPL-motors were disassociated from the PLL surface by pipetting gently and repeatedly, followed by two PBS washes. The micromotors were suspended in PBS and stored at 4°C until use.

### Fabrication of non-JPLs

The reactions were performed in 1.7-ml Eppendorf tubes (Corning). Platelets were modified with the same chemicals at the same ratios as the fabrication of JPL-motors. The resulting non-JPLs were dispersed in PBS and stored at 4°C until use.

### Characterization of JPL-motors

The Janus coating of urease onto the platelet surface was characterized by the fluorescent imaging of Cy5. All the bright-field, fluorescence, and merged images were captured using an EVOS FL microscope with a 40× objective. Flow cytometry analyses were also applied to evaluate the successful modification and binding efficiency of Cy5-labeled urease using a Becton Dickinson FACSCanto II flow cytometer. PLs, platelet modification without using biotinylated urease or streptavidin, were used as control experiments. P-selectin was selected to characterize the platelet activation. Resting platelets, PLs, and JPL-motors at a density of $10^6$/ml were all incubated with 5 μl of phycoerythrin-labeled P-selectin (BioLegend) for 30 min, after which they were washed with PBS three times before flow cytometry analysis.

To compare the protein profile of the platelets before and after modification, both JPL-motors and PLs were centrifuged and resuspended in 1× PBS three times. Then, a BCA assay (Thermo Fisher Scientific) was used to quantify the membrane proteins on the JPL-motors as per the manufacturer's instructions. Gel electrophoresis followed by protein staining with Coomassie blue was also performed. PLs and JPL-motors containing equivalent total proteins were prepared in lithium dodecyl sulfate sample loading buffer (Invitrogen). The samples were then separated on a 4 to 12% bis-tris 17-well Mini Gel in Mops running buffer using a Novex XCell SureLock electrophoresis system (Life Technologies). Last, the protein columns were stained with Coomassie blue according to the manufacturer's protocol.

### Propulsion study

All the experiments were performed in PBS solution by mixing JPL-motors with urea solution at the desired concentrations. A cover slide was applied to avoid the drifting effect. The propulsion videos were captured using an inverted optical microscope (Eclipse Ti-S/L100, Nikon Instruments Inc.) with a 40× microscope objective. The propulsion analysis was performed with NIS-Elements AR 3.2 software. The simulated urine was prepared according to the protocol described in a previous report (*63*). Briefly, 0.073 g of NaCl, 0.040 g of KCl, 0.028 g of $CaCl_2{\cdot}2H_2O$, 0.056 g of $Na_2SO_4$, 0.035 g of $KH_2PO_4$, 0.025 g of $NH_4Cl$, and 0.15 g of urea were added to 25 ml of deionized water to obtain the simulated urine with 100 mM urea for investigating the propulsion behavior of JPL-motors in this medium.

### Binding of JPL-motors with bacteria and cancer cells

SEM images of JPL-motors binding with *E. coli* and MDA-MB-231 breast cancer cells were performed on an Apreo high-resolution instrument (FEI, Hillsboro, OR, USA) with an accelerating voltage of 10 kV. Binding was further confirmed by fluorescent imaging. The breast cancer cell, MDA-MB-231, was labeled with Hoechst 33342 (Invitrogen), and the *E. coli* (DH5α) was labeled with DAPI (Sigma-Aldrich). All the bright-field, fluorescence, and merged images were captured using an EVOS FL microscope coupled with a 20× objective.

To explore the effect of urease modification on platelets' adhesion to cancer cells, PLs and RBCs were used as positive and negative controls, respectively. The JPL-motors, PLs, and RBCs at the cell concentration of $10^8$ cells/ml were all labeled with DiD dye (1 μg/ml) for 30 min at room temperature. Then, the resulting suspension was centrifuged (1500 rcf, 3 min) to remove the free dyes by washing three times with PBS. The binding assay was conducted by incubating the DiD-labeled JPL-motors, PLs, and RBCs with MDA-MB-231 cells at the ratio of 10:1 for 30 min at the room temperature, followed by flow cytometry analysis to quantify the binding efficiency to MDA-MB-231.

To quantify the specific binding of JPL-motors and PLs to *E. coli*, both JPL-motors and PLs ($10^{12}$ cells/ml) were first labeled with DiD (1 μg/ml) for 30 min at room temperature, followed by washing three times and centrifugation (1500 rcf, 3 min). *E. coli* ($3 \times 10^9$ cells/ml) was labeled with DAPI (1 μg/ml) for 30 min at room temperature. The free dye was then removed through three washing steps with centrifugation at 5900 rcf for 5 min. The DiD-labeled JPL-motors and PLs were incubated with *E. coli* at the ratio of 1:5 for 30 min at room temperature, followed by microscopy imaging. The percentage of JPL-motors or PLs that bind to *E. coli* was quantified by manually counting 10 representative images taken for each sample.

The binding efficiency of JPL-motors and PLs with *E. coli* and MDA-MB-231 cells in the presence of urea was also evaluated. JPL-motors and PLs ($10^{12}$ cells/ml) were first labeled with DiD (1 μg/ml), followed by washing steps to remove free dyes. DiD-labeled JPL-motors and PLs ($10^{12}$ cells/ml) were then mixed with bacteria ($3 \times 10^9$ cells/ml) at the ratio of 1:15 and cancer cells ($10^5$ cells/ml) at the ratio of 1:5 for different periods in the presence of 100 mM urea. The resulting aggregates of platelets and *E. coli* were separated by centrifugation at 600 rcf for 3 min and washed with PBS two times. The aggregates of platelets and MDA-MB-231 cells were collected with a 3-min centrifugation at 100 rcf, followed by two PBS washes. The aggregates were suspended in PBS and transferred to a 96-well plate. The binding efficiency was determined by the fluorescent intensity of DiD, measured with a BioTek Synergy Mx microplate reader.

### DOX or Cip loading and release from JPL-motors

A total of 200 μl of DOX (Sigma-Aldrich) or Cip (Sigma-Aldrich), with different initial drug input concentrations (DOX input: 3.125, 6.25, 12.5, 25, and 50 μM; Cip input: 1.563, 3.125, 6.25, 12.5, and 25 μg/ml), was incubated with JPL-motors or PLs ($10^8$ cells) at 37°C for 1 hour, followed by removal of the free drug by two washes at 2300 rcf for 3 min. Then, drug-loaded JPL-motors were suspended in 200 μl of PBS for further use. The concentration of DOX (Ex/Em = 488/594 nm) and Cip (Ex/Em = 280/425 nm) were quantified by their fluorescent intensities measured by a BioTek Synergy Mx microplate reader. The loading efficiency was determined as the amount of the loaded drug divided by the drug input. The drug release was performed with 200 μl of fresh JPL-motor loaded with DOX or Cip at pH 5.0 or 7.4.

### In vitro anticancer activity of DOX-loaded JPL-motors

The MDA-MB-231 cells ($10^6$ cells) were first incubated with PBS or urea only (negative controls), free DOX, PL-DOX, and JPL-motor–DOX at the same DOX concentration of 10 μM with different urea concentrations (0, 50, and 100 mM) for 10 min in 1.7-ml Eppendorf tubes. Then, the cancer cells were isolated by centrifugation at 100 rcf for 3 min and washed two times with PBS. The collected cells were further incubated with fresh DMEM in a 96-well plate at 37°C for 24 hours. After that, an MTS (Promega) [3-(4,5-dimethylthiazol-2-yl)-5-(3-carboxymethoxyphenyl)-2-(4-sulfophenyl)-2H-tetrazolium] assay was conducted to evaluate cell viability based on the manufacturer's protocol. The absorbance at 490 nm was read using a BioTek Synergy Mx microplate reader.

### In vitro antibacterial activity of Cip-loaded JPL-motors

Typically, *E. coli* ($2 \times 10^6$ CFU/ml) was mixed with PBS or urea only (negative controls), free Cip, PL-Cip, and JPL-motor–Cip at the same Cip concentration of 10 μg/ml with different urea concentrations (0, 50, and 100 mM) for 5 min. Then, the bacteria were collected by centrifugation at 600 rcf for 3 min and washed two times with PBS. The bacteria were then transferred to 1 ml of LB broth (Luria-Bertani, BD Difco) and cultured for 24 hours at 37°C. Last, the bacterial colonies were counted by measuring their absorbance at 600 nm ($OD_{600}$).

## SUPPLEMENTARY MATERIALS

robotics.sciencemag.org/cgi/content/full/5/43/eaba6137/DC1

Fig. S1. Microscopy images of JPL-motors with Cy5-labeled urease on the surface of a well plate before pipetting.
Fig. S2. Propulsion performance of PLs in various media containing 100 mM urea.
Fig. S3. Propulsion performance of JPL-motors after 30 min at a urea concentration of 100 mM compared with the motion at initial stage.
Fig. S4. Characterizations of non-JPLs with Cy5-labeled urease.
Fig. S5. Representative flow cytometry histograms of MDA-MB-231 cells incubated for 30 min with DiD-labeled JPL-motors (orange), PLs (cyan), and RBCs (blue).
Fig. S6. Microscopy images of DOX-loaded JPL-motors.
Fig. S7. Loading amount of JPL-motors and PLs at various DOX initial inputs.
Fig. S8. Propulsion performance of JPL-motors with and without DOX loading at a urea concentration of 100 mM.
Fig. S9. SEM image of the binding of JPL-motors to *E. coli* bacteria.
Fig. S10. Comparison of the binding affinity of PLs or JPL-motors to *E. coli*.
Fig. S11. Loading amount of JPL-motors and PLs at various Cip initial inputs.
Fig. S12. Propulsion performance of JPL-motors with and without Cip loading in the presence of 100 mM urea.
Table S1. Quantifications of protein content of PLs, platelets with Janus modification of sulfo-NHS-biotin and streptavidin (JPL-strep), and JPL-motors with the same cell concentration of $5 \times 10^{11}$ cells/ml.
Movie S1. Propulsion performance of JPL-motors in various urea concentrations.
Movie S2. Propulsion performance of multiple JPL-motors in the presence of 50 mM urea.
Movie S3. Propulsion performance of JPL-motors in various media at a urea concentration of 100 mM.
Movie S4. Propulsion performance of PLs in various media containing 100 mM urea.
Movie S5. Propulsion performance of JPL-motors after 30 min at a urea concentration of 100 mM compared with that at the initial stage.
Movie S6. Propulsion performance of non-JPLs at various urea concentrations.
Movie S7. Motion comparison of JPL-motors with and without DOX loading at a urea concentration of 100 mM.
Movie S8. Motion comparison of JPL-motors with and without Cip loading at a urea concentration of 100 mM.

## REFERENCES AND NOTES

1. F. Pierigè, S. Serafini, L. Rossi, M. Magnani, Cell-based drug delivery. *Adv. Drug Deliv. Rev.* **60**, 286–295 (2008).

2. L. A. L. Fliervoet, E. Mastrobattista, Drug delivery with living cells. *Adv. Drug Deliv. Rev.* **106**, 63–72 (2016).
3. T. Burnouf, P.-A. Burnouf, Y.-W. Wu, E.-Y. Chuang, L.-S. Lu, H. Goubran, Circulatory-cell-mediated nanotherapeutic approaches in disease targeting. *Drug Discov. Today* **23**, 934–943 (2018).
4. J. W. Semple, J. E. Italiano Jr., J. Freedman, Platelets and the immune continuum. *Nat. Rev. Immunol.* **11**, 264–274 (2011).
5. S. Sarkar, M. A. Alam, J. Shaw, A. Kr. Dasgupta, Drug delivery using platelet cancer cell interaction. *Pharm. Res.* **30**, 2785–2794 (2013).
6. P. Xu, H. Zuo, B. Chen, R. Wang, A. Ahmed, Y. Hu, J. Ouyang, Doxorubicin-loaded platelets as a smart drug delivery system: An improved therapy for lymphoma. *Sci. Rep.* **7**, 42632 (2017).
7. Z. Li, S. Hu, K. Cheng, Platelets and their biomimetics for regenerative medicine and cancer therapies. *J. Mater. Chem. B* **6**, 7354–7365 (2018).
8. M. Demers, D. D. Wagner, Targeting platelet function to improve drug delivery. *Oncoimmunology* **1**, 100–102 (2012).
9. Q. Shi, R. R. Montgomery, Platelets as delivery systems for disease treatments. *Adv. Drug Deliv. Rev.* **62**, 1196–1203 (2010).
10. A. M. Fennimore, T. D. Yuzvinsky, W.-Q. Han, M. S. Fuhrer, J. Cumings, A. Zettl, Rotational actuators based on carbon nanotubes. *Nature* **424**, 408–410 (2003).
11. J. Xi, J. J. Schmidt, C. D. Montemagno, Self-assembled microdevices driven by muscle. *Nat. Mater.* **4**, 180–184 (2005).
12. B. Esteban-Fernández de Ávila, P. Angsantikul, J. Li, M. Angel Lopez-Ramirez, D. E. Ramírez-Herrera, S. Thamphiwatana, C. Chen, J. Delezuk, R. Samakapiruk, V. Ramez, M. Obonyo, L. Zhang, J. Wang, Micromotor-enabled active drug delivery for in vivo treatment of stomach infection. *Nat. Commun.* **8**, 272 (2017).
13. J. T. Kim, U. Choudhury, H.-H. Jeong, P. Fischer, Nanodiamonds that swim. *Adv. Mater.* **29**, 1701024 (2017).
14. J. Li, B. Esteban-Fernández de Ávila, W. Gao, L. Zhang, J. Wang, Micro/nanorobots for biomedicine: Delivery, surgery, sensing, and detoxification. *Sci. Robot.* **2**, eaam6431 (2017).
15. Z. Wu, J. Troll, H.-H. Jeong, Q. Wei, M. Stang, F. Ziemssen, Z. Wang, M. Dong, S. Schnichels, T. Qiu, P. Fischer, A swarm of slippery micropropellers penetrates the vitreous body of the eye. *Sci. Adv.* **4**, eaat4388 (2018).
16. W. Wang, W. Duan, A. Sen, T. E. Mallouk, Catalytically powered dynamic assembly of rod-shaped nanomotors and passive tracer particles. *Proc. Natl. Acad. Sci. U.S.A.* **110**, 17744–17749 (2013).
17. V. Magdanz, M. Medina-Sánchez, L. Schwarz, H. Xu, J. Elgeti, O. G. Schmidt, Spermatozoa as functional components of robotic microswimmers. *Adv. Mater.* **29**, 1606301 (2017).
18. F. Peng, Y. Tu, D. A. Wilson, Micro/nanomotors towards in vivo application: Cell, tissue and biofluid. *Chem. Soc. Rev.* **46**, 5289–5310 (2017).
19. K. Kim, J. Guo, Z. Liang, D. Fan, Artificial micro/nanomachines for bioapplications: Biochemical delivery and diagnostic sensing. *Adv. Funct. Mater.* **28**, 1705867 (2018).
20. X. Yan, Q. Zhou, M. Vincent, Y. Deng, J. Yu, J. Xu, T. Xu, T. Tang, L. Bian, Y.-X. J. Wang, K. Kostarelos, L. Zhang, Multifunctional biohybrid magnetite microrobots for imaging-guided therapy. *Sci. Robot.* **2**, eaaq1155 (2017).
21. M. Pal, N. Somalwar, A. Singh, R. Bhat, S. M. Eswarappa, D. K. Saini, A. Ghosh, Maneuverability of magnetic nanomotors inside living cells. *Adv. Mater.* **30**, e1800429 (2018).
22. F. Zhang, R. Mundaca-Uribe, H. Gong, B. Esteban-Fernández de Ávila, M. Beltrán-Gastélum, E. Karshalev, A. Nourhani, Y. Tong, B. Nguyen, M. Gallot, Y. Zhang, L. Zhang, J. Wang, A macrophage-magnesium hybrid biomotor: Fabrication and characterization. *Adv. Mater.* **31**, e1901828 (2019).
23. H. Wang, M. Pumera, Micro/nanomachines and living biosystems: From simple interactions to microcyborgs. *Adv. Funct. Mater.* **28**, 1705421 (2018).
24. L. Schwarz, M. Medina-Sánchez, O. G. Schmidt, Hybrid biomicromotors. *Appl. Phys. Rev.* **4**, 031301 (2017).
25. C. Gao, Z. Lin, X. Lin, Q. He, Cell membrane–camouflaged colloid motors for biomedical applications. *Adv. Therap.* **1**, 1800056 (2018).
26. X. Z. Chen, B. Jang, D. Ahmed, C. Hu, C. De Marco, M. Hoop, F. Mushtaq, B. J. Nelson, S. Pané, Small-scale machines driven by external power sources. *Adv. Mater.* **30**, e1705061 (2018).
27. Z. Wu, T. Li, J. Li, W. Gao, T. Xu, C. Christianson, W. Gao, M. Galarnyk, Q. He, L. Zhang, J. Wang, Turning erythrocytes into functional micromotors. *ACS Nano* **8**, 12041–12048 (2014).
28. S. Jeon, S. Kim, S. Ha, S. Lee, E. Kim, S. Y. Kim, S. H. Park, J. H. Jeon, S. W. Kim, C. Moon, B. J. Nelson, J.-y. Kim, S.-W. Yu, H. Choi, Magnetically actuated microrobots as a platform for stem cell transplantation. *Sci. Robot.* **4**, eaav4317 (2019).
29. Z. Lin, X. Fan, M. Sun, C. Gao, Q. He, H. Xie, Magnetically actuated peanut colloid motors for cell manipulation and patterning. *ACS Nano* **12**, 2539–2545 (2018).
30. J. Li, X. Li, T. Luo, R. Wang, C. Liu, S. Chen, D. Li, J. Yue, S.-h. Cheng, D. Sun, Development of a magnetic microrobot for carrying and delivering targeted cells. *Sci. Robot.* **3**, eaat8829 (2018).
31. Z. Wu, B. Esteban-Fernández de Ávila, A. Martín, C. Christianson, W. Gao, S. K. Thamphiwatana, A. Escarpa, Q. He, L. Zhang, J. Wang, RBC micromotors carrying multiple cargos towards potential theranostic applications. *Nanoscale* **7**, 13680–13686 (2015).
32. K. Villa, L. Krejčová, F. Novotný, Z. Heger, Z. Sofer, M. Pumera, Cooperative multifunctional self-propelled paramagnetic microrobots with chemical handles for cell manipulation and drug delivery. *Adv. Funct. Mater.* **28**, 1804343 (2018).
33. Y. Alapan, O. Yasa, O. Schauer, J. Giltinan, A. F. Tabak, V. Sourjik, M. Sitti, Soft erythrocyte-based bacterial microswimmers for cargo delivery. *Sci. Robot.* **3**, eaar4423 (2018).
34. I.-A. Pavel, A.-I. Bunea, S. David, S. Gáspár, Nanorods with biocatalytically induced self-electrophoresis. *ChemCatChem* **6**, 866–872 (2014).
35. P. S. Schattling, M. A. Ramos-Docampo, V. Salgueiriño, B. Städler, Double-fueled janus swimmers with magnetotactic behavior. *ACS Nano* **11**, 3973–3983 (2017).
36. T. Patiño, X. Arqué, R. Mestre, L. Palacios, S. Sánchez, Fundamental aspects of enzyme-powered micro-and nanoswimmers. *Acc. Chem. Res.* **51**, 2662–2671 (2018).
37. K. K. Dey, X. Zhao, B. M. Tansi, W. J. Méndez-Ortiz, U. M. Córdova-Figueroa, R. Golestanian, A. Sen, Micromotors powered by enzyme catalysis. *Nano Lett.* **15**, 8311–8315 (2015).
38. S. Keller, S. P. Teora, G. X. Hu, M. Nijemeisland, D. A. Wilson, High-throughput design of biocompatible enzyme-based hydrogel microparticles with autonomous movement. *Angew. Chem. Int. Ed.* **57**, 9814–9817 (2018).
39. X. Arqué, A. Romero-Rivera, F. Feixas, T. Patiño, S. Osuna, S. Sánchez, Intrinsic enzymatic properties modulate the self-propulsion of micromotors. *Nat. Commun.* **10**, 2826 (2019).
40. P. Schattling, B. Thingholm, B. Städler, Enhanced diffusion of glucose-fueled Janus particles. *Chem. Mater.* **27**, 7412–7418 (2015).
41. A. C. Hortelão, T. Patiño, A. Perez-Jiménez, À. Blanco, S. Sánchez, Enzyme-powered nanobots enhance anticancer drug delivery. *Adv. Funct. Mater.* **28**, 1705086 (2018).
42. A. C. Hortelão, R. Carrascosa, N. Murillo-Cremaes, T. Patiño, S. Sánchez, Targeting 3d bladder cancer spheroids with urease-powered nanomotors. *ACS Nano* **13**, 429–439 (2018).
43. T. Patiño, N. Feiner-Gracia, X. Arqué, A. Miguel-López, A. Jannasch, T. Stumpp, E. Schäffer, L. Albertazzi, S. Sánchez, Influence of enzyme quantity and distribution on the self-propulsion of non-Janus urease-powered micromotors. *J. Am. Chem. Soc.* **140**, 7896–7903 (2018).
44. J. Park, B. Andrade, Y. Seo, M.-J. Kim, S. C. Zimmerman, H. Kong, Engineering the surface of therapeutic "living" cells. *Chem. Rev.* **118**, 1664–1690 (2018).
45. S. Abbina, E. M. J. Siren, H. Moon, J. N. Kizhakkedathu, Surface engineering for cell-based therapies: Techniques for manipulating mammalian cell surfaces. *ACS Biomater Sci. Eng.* **4**, 3658–3677 (2017).
46. J. Niu, D. J. Lunn, A. Pusuluri, J. I. Yoo, M. A. O'Malley, S. Mitragotri, H. T. Soh, C. J. Hawker, Engineering live cell surfaces with functional polymers via cytocompatible controlled radical polymerization. *Nat. Chem.* **9**, 537–545 (2017).
47. D. G. Menter, S. C. Tucker, S. Kopetz, A. K. Sood, J. D. Crissman, K. V. Honn, Platelets and cancer: A casual or causal relationship: Revisited. *Cancer Metastasis Rev.* **33**, 231–269 (2014).
48. O. Garraud, Editorial: Platelets as immune cells in physiology and immunopathology. *Front. Immunol.* **6**, 274 (2015).
49. S. W. Kerrigan, D. Cox, Platelet–bacterial interactions. *Cell. Mol. Life Sci.* **67**, 513–523 (2010).
50. H. Lu, L. Guo, N. Kawazoe, T. Tateishi, G. Chen, Effects of poly(L-lysine), poly(acrylic acid) and poly(ethylene glycol) on the adhesion, proliferation and chondrogenic differentiation of human mesenchymal stem cells. *J. Biomater. Sci. Polym. Ed.* **20**, 577–589 (2009).
51. J. R. Howse, R. A. L. Jones, A. J. Ryan, T. Gough, R. Vafabakhsh, R. Golestanian, Self-motile colloidal particles: From directed propulsion to random walk. *Phys. Rev. Lett.* **99**, 048102 (2007).
52. G. Dunderdale, S. Ebbens, P. Fairclough, J. Howse, Importance of particle tracking and calculating the mean-squared displacement in distinguishing nanopropulsion from other processes. *Langmuir* **28**, 10997–11006 (2012).
53. J. Suchanski, J. Grzegrzolka, T. Owczarek, P. Pasikowski, A. Piotrowska, B. Kocbach, A. Nowak, P. Dziegiel, A. Wojnar, M. Ugorski, Sulfatide decreases the resistance to stress-induced apoptosis and increases P-selectin-mediated adhesion: A two-edged sword in breast cancer progression. *Breast Cancer Res.* **20**, 133 (2018).
54. P. Mohan, N. Rapoport, Doxorubicin as a molecular nanotheranostic agent: Effect of doxorubicin encapsulation in micelles or nanoemulsions on the ultrasound-mediated intracellular delivery and nuclear trafficking. *Mol. Pharm.* **7**, 1959–1973 (2010).
55. S. V. Blokhina, A. V. Sharapova, M. V. Ol'khovich, T. V. Volkova, G. L. Perlovich, Solubility, lipophilicity and membrane permeability of some fluoroquinolone antimicrobials. *Eur. J. Pharm. Sci.* **93**, 29–37 (2016).
56. M. Banerjee, S. W. Whiteheart, The ins and outs of endocytic trafficking in platelet functions. *Curr. Opin. Hematol.* **24**, 467–474 (2017).
57. E. Baumann, W. Linß, M. Fröhner, G. Stoya, W. Richter, Ph-induced denaturation of spectrin changes the interaction of membrane proteins in erythrocyte ghosts. Biochemical and electron microscopic evidence. *Ann. Anat.* **176**, 93–99 (1994).

58. J. R. Fitzgerald, T. J. Foster, D. Cox, The interaction of bacterial pathogens with platelets. *Nat. Rev. Microbiol.* **4**, 445–457 (2006).
59. C. N. Watson, S. W. Kerrigan, D. Cox, I. R. Henderson, S. P. Watson, M. Arman, Human platelet activation by *Escherichia coli*: Roles for fcγriia and integrin αiibβ3. *Platelets* **27**, 535–540 (2016).
60. R. J. Fass, Efficacy and safety of oral ciprofloxacin for treatment of serious urinary tract infections. *Antimicrob. Agents Chemother.* **31**, 148–150 (1987).
61. F. Mou, C. Chen, H. Ma, Y. Yin, Q. Wu, J. Guan, Self-propelled micromotors driven by the magnesium–water reaction and their hemolytic properties. *Angew. Chem. Int. Ed.* **52**, 7208–7212 (2013).
62. A. Somasundar, S. Ghosh, F. Mohajerani, L. N. Massenburg, T. Yang, P. S. Cremer, D. Velegol, A. Sen, Positive and negative chemotaxis of enzyme-coated liposome motors. *Nat. Nanotechnol.* **14**, 1129–1134 (2019).
63. P. Batista Deroco, F. Campanhã Vicentini, G. Gabriel Oliveira, R. C. Rocha-Filho, O. Fatibello-Filho, Square-wave voltammetric determination of hydroxychloroquine in pharmaceutical and synthetic urine samples using a cathodically pretreated boron-doped diamond electrode. *J. Electroanal. Chem.* **719**, 19–23 (2014).


**Acknowledgments:** We acknowledge the suggestions of fluorescence images from J. Zhang and T. Sun. **Funding:** This work was supported by the Defense Threat Reduction Agency Joint Science and Technology Office for Chemical and Biological Defense (grant numbers HDTRA1-14-1-0064 and HDTRA1-13-10002) and National Natural Science Foundation of China (grant numbers 21890740 and 21727815). S.T. acknowledges the China Scholarship Council (CSC) for the financial support. **Author contributions:** All authors contributed to the writing of the manuscript. All authors have given approval to the final version of the manuscript. **Competing interests:** The authors declare that they have no competing financial interests. **Data and materials availability:** All data needed to evaluate the study are in the paper or in the Supplementary Materials.

Submitted 18 December 2019
Accepted 30 April 2020
Published 10 June 2020
10.1126/scirobotics.aba6137

**Citation:** S. Tang, F. Zhang, H. Gong, F. Wei, J. Zhuang, E. Karshalev, B. Esteban-Fernández de Ávila, C. Huang, Z. Zhou, Z. Li, L. Yin, H. Dong, R. H. Fang, X. Zhang, L. Zhang, J. Wang, Enzyme-powered Janus platelet cell robots for active and targeted drug delivery. *Sci. Robot.* **5**, eaba6137 (2020).

Science Robotics

# Enzyme-powered Janus platelet cell robots for active and targeted drug delivery

Songsong Tang, Fangyu Zhang, Hua Gong, Fanan Wei, Jia Zhuang, Emil Karshalev, Berta Esteban-Fernández de Ávila, Chuying Huang, Zhidong Zhou, Zhengxing Li, Lu Yin, Haifeng Dong, Ronnie H. Fang, Xueji Zhang, Liangfang Zhang, and Joseph Wang

*Sci. Robot.* **5** (43), eaba6137. DOI: 10.1126/scirobotics.aba6137







*Science Robotics* (ISSN 2470-9476) is published by the American Association for the Advancement of Science. 1200 New York Avenue NW, Washington, DC 20005. The title *Science Robotics* is a registered trademark of AAAS.